Physicochem. Probl. Miner. Process., 61(6), 2025, 215142

http://www.journalssystem.com/ppmp

Physicochemical Problems of Mineral Processing

ISSN 1643-1049

Study on fluidization mechanisms and characteristics of turbulence particle fluidized bed in mineralization

Zhengjun Zhu [1], Fan Wu [1], Huilin Xu [1], An Ping [1], Yingxiang Shi [1], Zhongkuan Wei [1], Jixuan Gao [1], Yanfeng Li [2]

[1] China Coal (Tianjin) Design Engineering Co., Ltd., Tianjin 300120, China

[2] School of Chemical Engineering and Technology, China University of Mining and Technology, Xuzhou 221112, China

Corresponding author: ap10486@163.com (An Ping)

Abstract: This study investigates the fluidization behavior of a turbulence-regulated particle fluidized bed, focusing on its application to flotation processes. Key variables – including particle size, gas velocity, and bed height – were examined to assess their effects on pressure drop, expansion ratio, volatility, and porosity. Results show that the minimum fluidization velocity decreases as gas velocity and particle size increase. A comprehensive bed flow model was developed, utilizing multiple linear regression and dimensionless numbers to characterize the system's hydrodynamics. The models accurately predict fluctuation ratio, expansion ratio, and porosity across different operating conditions. Additionally, the relationship between bubble diameter and expansion parameters was explored, revealing that bed height significantly influences bubble size behavior. These findings offer practical insights for optimizing industrial fluidized bed performance, especially in flotation systems, and lay the groundwork for future experimental research.

Keywords: floating, three-phase fluidized bed, fluid dynamics, gas content ratio, bubble surface area flux

1. Introduction

A fluidized bed involves solid particles suspended by an upward flow of multiple phases. Reese et al. (Jo et al., 2022) explored its use in industrial contexts, especially focusing on three-phase fluidized systems. These systems have proven significant advantages, leading to their widespread application across various fields including chemical engineering, physical processes, and biochemical research (Abu Khalifeh et al., 2021; Jena et al., 2008b). Since the flotation column was introduced, it has seen substantial development due to its ability to handle fine particles efficiently and its broad applicability in diverse scientific areas (Bhunia et al., 2015; Cai et al., 2017; Fan et al., 2013; Lei et al., 2020; Venkatraman, 1996). Essential gas-related parameters, including gas retention and bubble diameter, are vital for assessing flotation effectiveness, as they directly influence the performance of flotation columns (Li et al., 2008). Therefore, understanding these parameters thoroughly is crucial for efficient operation management and diagnosis of flotation columns. Many scholarly works have addressed these gas-phase metrics (Jena et al., 2008a; Lefebvre et al., 2007; Sobrino et al., 2009; Wang et al., 2003). Research on gas dynamics in flotation columns dates back to the late 1900s when Yianatos used the impulse response technique to examine the residence time distribution of tracer gases (Yianatos et al., 2017). Later, Ityokumbul introduced a simple method for measuring bubble size within flotation systems (Pan et al., 2018). Gorain further contributed by developing an empirical formula for bubble surface area flux based on extensive pilot-scale testing in mechanical flotation units (Gorain et al., 1999). Sarhan applied computational fluid dynamics (CFD) to study gas retention and bubble movement in three-phase flotation systems (Sarhan et al., 2017), while Wang utilized CFD simulations for comprehensive flotation modeling (Wang et al., 2018). Ravichandran aimed to improve flotation performance by refining gas parameters to increase gas hold-up (Ravichandran et al., 2013). However, detailed analysis of

DOI: 10.37190/ppmp/215142

parameters like bubble diameter, gas hold-up, and bubble surface area flux within flotation columns remains limited.

The shape of a bubble is mainly affected by five key physical parameters. Descriptions of bubble form are usually expressed using several dimensionless parameters (Ellingsen and Risso, 2001; Liu et al., 2021). Among these methods, the aspect ratio is commonly used, which refers to the ratio between a bubble's short and long axes—it's a straightforward and effective way to describe bubble shape. Recently, much effort has been focused on studying the geometry of individual bubbles. Experimental results indicate that dimensionless numbers offer a reliable way to accurately describe bubble shape features (Aoyama et al., 2016; Shi et al., 2018). However, Los-(Loth, 2008) questioned whether these findings can be widely applied, pointing out the difficulties of using single-bubble experiments for two-phase or multiphase systems. These challenges come from variations in liquid flow behavior, phase interactions, and forces between bubbles, all of which impact bubble shape. Liu et al. (Liu et al., 2021) found that as bubble size increases, the aspect ratio tends to level off, which is different from what single-bubble correlation models predict, suggesting an inverse relationship. Additionally, Bessani and Inzoli (Besagni and Inzoli, 2019) highlighted that the arrangement of bubble clusters is closely related to specific operational parameters.

Research on fluidized bed behavior is a branch of fluid dynamics that mainly focuses on pressure drop and expansion parameters such as volatility, bed expansion, and void fraction (Pan et al., 2018). Examining these properties and developing flow models are crucial for evaluating the efficiency of industrial processes and designing system parameters. This chapter emphasizes studying the fluidization characteristics of fluidized beds, including the mechanisms of three-phase regions and the development of flow models. The goal is to gain a better understanding of flotation equipment performance and bubble formation mechanisms, laying the foundation for future experimental research.

2. Materials and methods

The fluidized bed expansion characteristic parameters, including bed volatility, bed expansion, and bed voidness, are calculated using the following equations.

$$r = \frac{h_{max}}{h_{\min}} \tag{1}$$

$$R = \frac{h_{max}+h_{\min}}{2H_s} \tag{2}$$

$$\varepsilon = 1 - \frac{M_S/\rho_S}{A\cdot(h_{\max}+h_{\min})/2} \tag{3}$$

The data for the highest and lowest points of the fluidized bed were obtained, for example, by using Fig. 1. The pressure drop across the bed is an important hydrodynamic indicator in three-phase fluidized systems, indicating whether steady-state conditions are reached. Sivaish (Sivaiah and Majumder, 2013) formulated an equation to describe the overall pressure drop in vertical systems as follows. $\Delta P = \Delta P_g + \Delta P_f + \Delta P_a$, where ΔP indicates the overall pressure drop, with ΔP_g representing the static head from gravity, ΔP_f the loss due to friction, and ΔP_a the acceleration component caused by

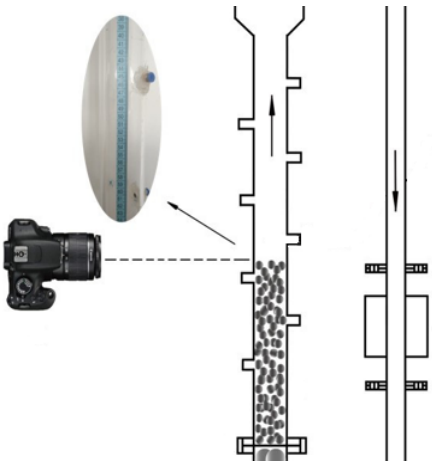

Fig. 1. Schematic of bed height data acquisition

changes in velocity; neglecting wall–solid friction, solid particles become fluidized once the product of the bed pressure drop and cross-sectional area is fully converted into drag from the gas–liquid mixture, while fluctuations in the bed pressure drop are directly controlled by the total fluid mass within the column.

3. Results and discussion

3.1. Turbulence regulation of pressure drop in granular fluidized bed beds

3.1.1. Study of the relationship between turbulence-regulated particle properties and bed pressure drop

As shown in Fig. 2, when the gas velocity is kept at 0 m/s and 3 mm glass beads are used as the solid-phase medium, the relationship between fluidized bed pressure drop and circulating flow rate is analyzed at different initial static bed heights. The results reveal that, for all three initial bed heights, the pressure drop increases sharply with rising apparent water velocity. Once the water velocity surpasses a certain threshold, the pressure drop levels off and fluctuates within a narrow range. This initial rapid increase in pressure is mainly caused by the higher water velocity: as the bed's porosity increases, solid particles begin to lift, allowing more liquid to occupy the void spaces. This results in a quick rise in the liquid volume within the bed and a corresponding increase in gravitational pressure. At the same time, increasing water velocity affects the flow rate, leading to a steeper rise in dynamic pressure drop. These two effects—gravitational and dynamic—are the main factors influencing the pressure changes. Since the solid phase consists of smooth glass beads and the liquid is of low viscosity, frictional pressure loss plays only a minor role in the overall pressure increase.

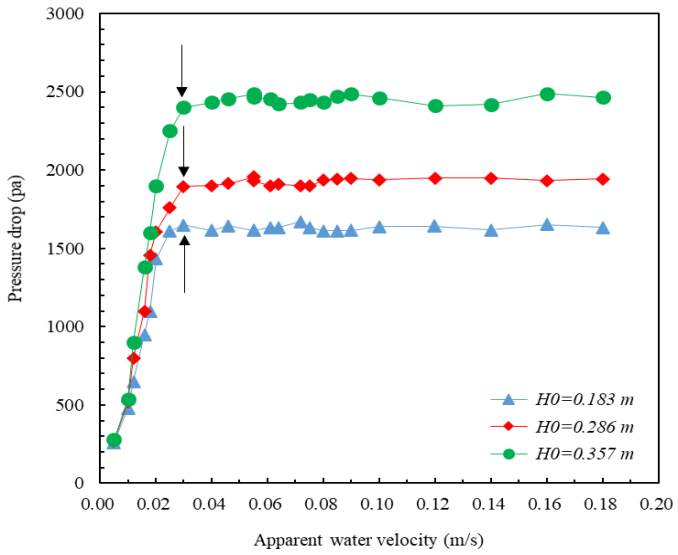

Fig. 2. Effect of apparent water velocity on bed pressure drop (Vg=0 m/s)

The reliable operation of gas–liquid–solid fluidized beds largely depends on accurately adjusting the minimum fluidization velocity, which is the liquid flow rate needed to start fluidization while keeping the gas supply constant. According to H.M (Jena et al., 2008), this parameter can be determined by analyzing the relationship between overall pressure drop and superficial liquid velocity at a fixed gas flow. Once fluidization is achieved, further increases in liquid flow cause minimal change in the total pressure drop. In this study, the black arrows in Figs. 2–4 point to the locations where the pressure drop stabilizes, with their X-axis positions indicating the minimum fluidization velocities. As shown in Fig. 2, when the superficial liquid velocity exceeds 0.03 m/s, the pressure drop curves for the three cases converge within a narrow range. According to the theory of minimum fluidization velocity, the initial bed height—representing the solids mass—has little effect on the critical velocity when only one particle type is used. However, a taller initial bed still results in a higher pressure drop, primarily because of the increased solid mass per unit volume, which enhances the gravitational component of bed pressure.

Fig. 3 shows how the bed pressure drop reacts to changes in apparent water velocity, given an apparent gas velocity of 0.02 m/s and an initial static bed height of 0.357 m. The results demonstrate that, for all three particle sizes used as packing materials, the pressure drop increases as the apparent water velocity rises. This upward trend closely follows what is seen in Fig. 2: at lower water velocities, the pressure drop climbs quickly, while beyond a certain threshold velocity, it stabilizes within a narrow fluctuation range—indicating the bed has entered a fluidized state. Specifically, as the water velocity increases from a low value, the bed responds with a rapid rise in pressure drop until fluidization occurs, after which the changes become minimal. Additionally, according to the theory of minimum fluidization velocity, larger particle sizes require higher fluid velocities to reach fluidization. In other words, the bigger the particle diameter, the higher the minimum liquid velocity needed for the bed to become fluidized.

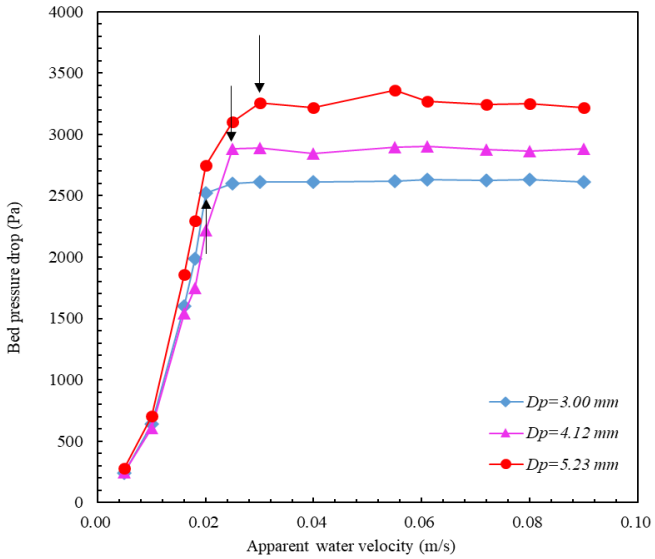

Fig. 3. Effect of filling particle size on bed pressure drop (Vg=0.02 m/s, H0=0.357 m)

3.1.2. Effect of apparent gas velocity on bed pressure drop

Fig. 4 shows the relationship between the bed pressure drop and the apparent liquid velocity at different filling volumes, with a starting static bed height of 0.286 m and 4.12 mm glass beads as the solid phase. The results show that increasing the circulation flow rate for each filling volume raises the pressure drop. When the liquid velocity exceeds a certain point, the pressure stabilizes and oscillates within a narrow range, indicating the start of fluidization. Additionally, the effect of superficial liquid velocity on bed pressure is strongly affected by gas flow: at lower gas rates, the pressure drop varies more significantly with increasing liquid velocity, while at higher gas rates, these fluctuations diminish, reflecting a more moderated response.

According to minimum fluidization theory, observations from Fig. 4 indicate that as gas velocity increases, the liquid velocity needed to start fluidization decreases, which is shown by the arrows shifting leftward in the figure. In other words, the minimum fluidization velocity drops with higher gas flow. This occurs because the increased gas throughput raises the gas fraction per unit volume and residence time in the bed, thereby reducing the overall density of the gas–liquid–solid mixture. Based on fluidization principles, when the product of pressure drop and cross-sectional area is fully converted into the drag exerted by the gas–liquid phases on the particles, fluidization occurs. Therefore, a decrease in mixture density lowers the required drag force, and with the column diameter remaining constant, a smaller pressure drop means less drag is needed. As a result, at higher gas velocities, the system needs a lower liquid velocity to achieve fluidization.

3.1.3. Analysis of how gas velocity influences the minimum fluidization threshold

Fig. 5 illustrates how the critical fluidization velocity varies with different gas flow rates when glass beads of various particle sizes are used as the filling medium, with an initial bed height of 0.286 m. As

shown in the figure, a clear pattern emerges: at a fixed gas flow rate, larger particles require a higher superficial liquid velocity to initiate fluidization. This indicates that bigger filling particles need more energy input to begin and maintain the fluidization process. In flotation experiments, therefore, using smaller particles as the filling medium can help reduce unnecessary energy consumption associated with fluidization. The overall goal is to minimize excess energy loss caused by fluidization of the filler particles.

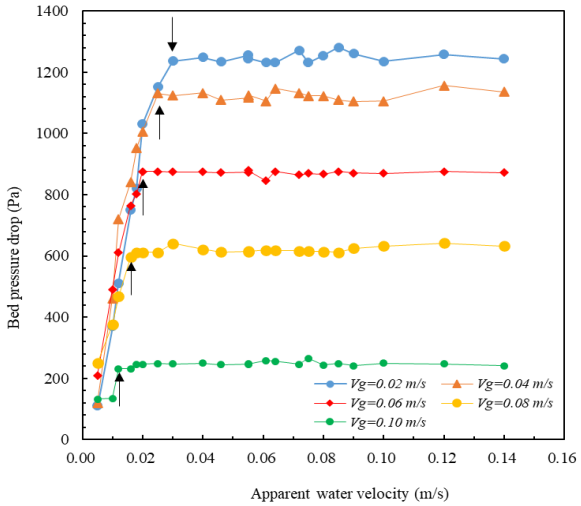

Fig. 4. Changes in bed pressure drop with apparent water velocity under varying gas velocities (Dp= 4.12 mm, H0= 0.286 m)

As shown in Fig. 5, for each tested particle size, the critical fluidization velocity nearly decreases linearly as the apparent gas flow increases. Table 1 summarizes the results of linear fits to the data in Fig. 5. From the final column, it is clear that the correlation coefficient R2 approaches 1 as particle size increases. This shows that, within the experimental range, larger particle diameters create a stronger linear relationship between critical fluidization velocity and apparent gas flow. In other words, the decrease in fluidization velocity tends to follow a linear trend more closely as particle size grows under controlled conditions.

Large particles exhibit a stronger linear correlation between minimum fluidization velocity and apparent gas velocity, with the R^2 value reaching 0.9984 for 5.23 mm particles. From a hydrodynamic perspective, large particles are more dominated by gravity, leading to a more stable balance between buoyancy and drag forces. They also have higher terminal settling velocities, making them less susceptible to local turbulent disturbances and resulting in more uniform flow state transitions, thus enhancing the linear relationship.

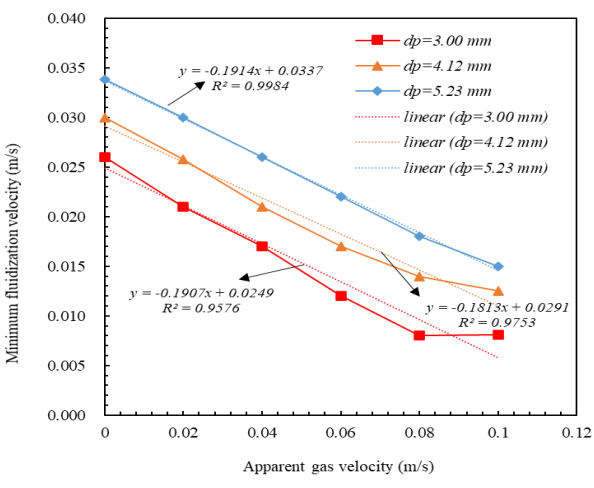

Fig. 5. Effect of gas flow rate on the critical fluidization velocity across particle sizes (H0=286 mm)

Table 1. Linear fitting data for minimum fluidization velocity at different particle sizes

Particle size (mm)	slope	intercept (the point at which a line crosses the x- or y-axis)	R2
3.00	0.1907	0.0249	0.9576
4.12	0.1813	0.0291	0.9753
5.23	0.1914	0.0337	0.9984

3.2. Turbulence regulation particle fluidized bed expansion characteristics research

3.2.1. Study of the relationship between turbulence-regulated particle properties and bed expansion properties

Fig. 6 illustrates how bed volatility reacts to changes in gas flow when the initial bed height is 0.290 m, using different types of filling particles. The results show that, for each particle size, bed volatility increases as apparent gas velocity rises. Specifically, beds packed with low-density glass beads experience more pronounced fluctuations, while those with high-density steel beads demonstrate more moderate variations. Under the same conditions of gas rate, liquid velocity, and initial bed height, it is evident that larger particle sizes lead to lower bed volatility. Conversely, when particle size remains constant, beds filled with lower-density materials tend to generate greater volatility during fluidization.

Figs. 7 and 8, like Fig. 6, show the relationship between bed expansion, bed voidage, and fluidization volume (shown by apparent gas velocity) under the same experimental conditions. The results indicate that when the initial bed height and liquid velocity stay constant, the three expansion parameters behave similarly. In this system, bed volatility, expansion ratio, and void fraction all increase as gas flow rises. However, the effect of initial bed height on expansion varies: bed volatility decreases with increasing initial bed height, while expansion increases accordingly, with little effect on void fraction.

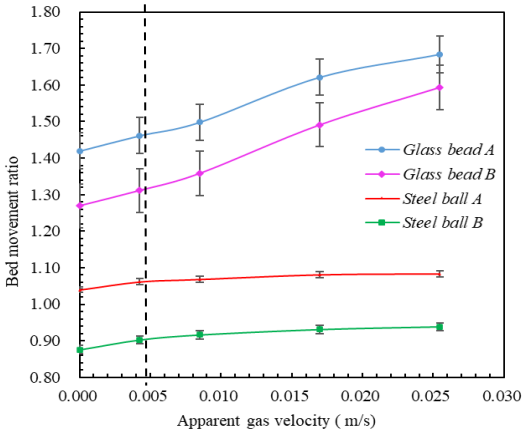

Fig. 6. Effect of filling particles on bed fluctuation ratio (H0=0.290 m, Vl=0.226 m/s)

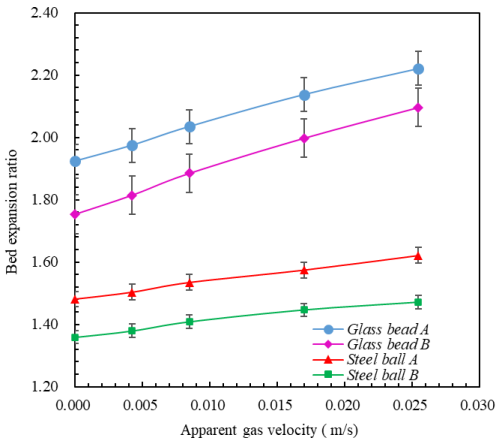

Fig. 7. Impact of filler particles on bed expansion ratio (H0=0.290 m, Vl=0.226 m/s)

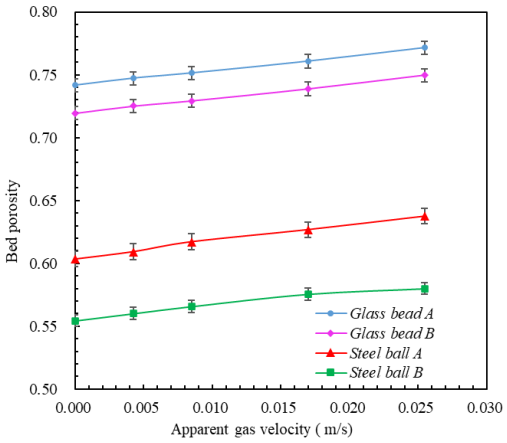

Fig. 8. Effect of filling particles on bed porosity (H0=0.290 m, Vl=0.226 m/s)

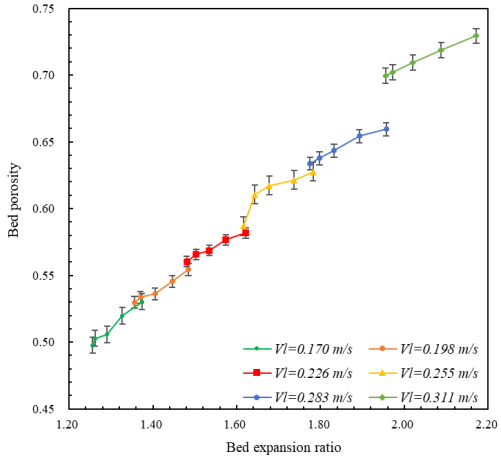

Fig. 9. Change in bed expansion ratio versus bed void (H0= 0.290 m, 0.004 m/s ≤ Vg ≤ 0.025 m/s)

Subsequent experiments showed that, under certain conditions, increasing the initial bed height leads to higher porosity in the fluidized bed. Based on the definitions in Equations 2 and 3 for expansion ratio and porosity, it can be inferred that these two parameters are positively related. Specifically, as the bed expansion ratio increases, porosity also rises, confirming a direct link between the degree of expansion and void fraction within the bed.

An increase in the initial bed height tends to raise both the expansion ratio and porosity at the same time, which appears inconsistent with some earlier results. Fig. 42 shows the relationship between porosity and expansion ratio at different gas velocities (0.004 m/s ≤ Vg ≤ 0.025 m/s), with an initial bed height of 0.290 m and varying liquid velocities. The results indicate that porosity increases as the expansion ratio expands. In related work, H.M designed a three-phase fluidized bed reactor for chemical applications, using hollow cylindrical particles as the solid phase. From his analysis, it was noted that the initial bed height had no effect on expansion. Therefore, he concluded that porosity is not directly determined by bed height but is influenced when bed height changes the expansion ratio.

3.2.2. Turbulence-regulated particle fluidized bed bed expansion model exploration

Based on the previous study results, the bubbles formed in the fluidized bed with 3 mm steel beads as filling particles are stable and exhibit relatively constant mobility. Therefore, the experimental data for 3 mm steel beads are selected as the basis for modelling the flow in this section.

The variation of flow parameters is mainly influenced by the nature of the filled particles, gas phase parameters, and liquid phase parameters. Indian scholar Dora (Dora et al., 2014) proposed a bed fluctuation rate model in the study of three-phase fluidization fluid dynamics of ternary mixtures, as shown in Eq. 4.

$$r = 0.002\left(\frac{G_f}{G_{mf}}\right)^{0.35} \cdot \left(\frac{H_s}{D_c}\right)^{-0.054} \cdot \left(\frac{D_{pav}}{D_c}\right)^{-1.65} \cdot \left(\frac{\rho_s}{\rho_f}\right)^{-0.108} \quad (4)$$

In this study, based on the experimental operating conditions and system parameters that influence the bed fluctuation ratio, the bed fluctuation ratio can be modeled as shown in Eq. 5.

$$r = f\left(V_l, V_g, V_{so}, H_o, D_c, V_l, \mu_l, \rho_l, g\right) \quad (5)$$

Based on the comparison between the quantitative analysis and the results of the fitting experiments, it was found that the fitting results were more accurate when Eq. 5 was transformed into the form of Eq. 6.

$$r = a \cdot [Re_l]^b \cdot \left[\frac{V_l}{V_{so}}\right]^c \cdot \left[\frac{V_g}{V_{so}}\right]^d \cdot \left(\frac{H_o}{D_c}\right)^e \quad (6)$$

The experimental data were substituted into Eq. 6, and the coefficients along with the constants were obtained through computer-based multiple linear regression, resulting in the fluctuation ratio model of the fluidized bed layer.

$$r = 0.565(Re_l)^{0.106} \cdot \left(\frac{V_l}{V_{so}}\right)^{-0.036} \cdot \left(\frac{V_g}{V_{so}}\right)^{0.015} \cdot \left(\frac{H_o}{D_c}\right)^{-0.174} \quad (7)$$

Fig. 10 shows a comparison between predicted and measured bed fluctuation ratios by model 7, while Table 2 presents the indices from multiple linear regression analysis. As seen in Fig. 10, the experimental data closely match the model predictions within the parameter ranges (0.169 ≤ Vl ≤ 0.311 m/s, 0.0042 ≤ Vg ≤ 0.025 m/s, 0.237 ≤ H0 ≤ 0.380 m). The new model has a correlation coefficient R=0.978 and an SSE value near zero, indicating it can accurately reflect changes in the fluidized bed fluctuation rate under experimental conditions.

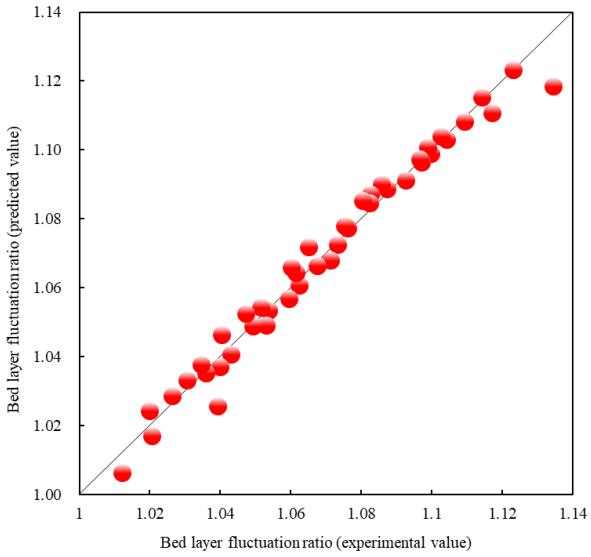

Fig. 10. Analysis of experimental and theoretical values of bed fluctuation ratio

Table 2. Indices of model 7 multiple linear regression analysis

Serial number	Project name (abbreviated)	numerical value
1	Mean Square Error (RMSE)	0.004451
2	Sum of residuals (SSE)	0.000872
3	Correlation coefficient (R)	0.988907
4	Square of correlation coefficient (R^2)	0.977938
5	Decision Coefficient (DC)	0.977937
6	chi-square (math.)	0.000406
7	F-statistic (F-statistic)	1861.803

For the bed expansion model, Indian scholar Dora (Dora et al., 2014) also proposed two mathematical models such as Eq. 8 and Eq. 9, which are similar in form to Model 4.

$$R = 8.00E-4\left(\frac{G_f}{G_{mf}}\right)^{0.787}\cdot\left(\frac{H_s}{D_c}\right)^{-0.444}\cdot\left(\frac{D_{pav}}{D_c}\right)^{-0.94} \tag{8}$$

$$R = 0.001\left(\frac{G_f}{G_{mf}}\right)^{0.58}\cdot\left(\frac{H_s}{D_c}\right)^{-0.735}\cdot\left(\frac{D_{pav}}{D_c}\right)^{-2.02}\cdot\left(\frac{\rho_s}{\rho_f}\right)^{-0.14} \tag{9}$$

Similar to how we modeled the bed fluctuation ratio, we apply the same approach to study the bed expansion ratio. Based on influencing factors, the bed expansion ratio can be expressed as Eq. 10.

$$R = f\left(V_l, V_g, V_{so}, H_o, D_c, g\right) \tag{10}$$

Based on the comparison of the results from the quantitative analysis and fitting experiments, it was observed that the fitting outcomes were more accurate when Eq. 10 was converted into the form of Eq. 11.

$$R = a\cdot[Fr_g]^b\cdot\left[\frac{V_l}{V_{so}}\right]^c\cdot\left[\frac{V_g}{V_{so}}\right]^d\cdot\left(\frac{H_o}{D_c}\right)^e \tag{11}$$

The coefficients and constants were obtained through computer-based multiple linear regression, using relevant experimental data as input, and then substituted into Eq. 11 to derive the fluidized bed layer expansion ratio model 12.

$$R = 3.13\left(Fr_g\right)^{0.412}\cdot\left(\frac{V_l}{V_{so}}\right)^{0.730}\cdot\left(\frac{V_g}{V_{so}}\right)^{-0.783}\cdot\left(\frac{H_o}{D_c}\right)^{0.209} \tag{12}$$

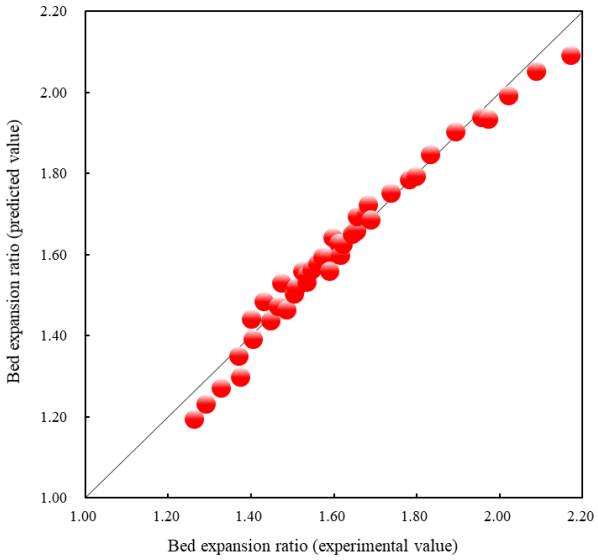

Fig. 11. Comparison of experimental and theoretical results for bed expansion ratio

Fig. 11 compares the predicted and measured values of bed expansion ratio from model 12, while Table 3 lists the indices derived from multiple linear regression. As shown in Figs. 5–11, within the parameter ranges, the experimental results closely match the model's predictions. The model demonstrates a strong fit, with a correlation coefficient R=0.975 and an SSE value approaching zero, confirming its accuracy in capturing bed swelling variation under experimental conditions.

Table 3. Indices for model 12 multiple linear regression analysis

Serial number	Project Name (abbreviated)	Numerical value
1	Mean Square Error (RMSE)	0.032546
2	Sum of residuals (SSE)	0.046606
3	Correlation coefficient (R)	0.987478
4	Square of correlation coefficient (R^2)	0.975113
5	Decision Coefficient (DC)	0.975103
6	chi-square (math.)	0.015310
7	F-statistic (F-statistic)	1645.673

For the study of bed void fraction modelling, model 13 was proposed in the study of the hydrodynamic properties of a three-phase fluidized bed with a hollow cylinder as the solid phase.

$$\varepsilon = 3.39{\varphi_s}^{-0.424} \cdot V_l^{0.271} V_g^{0.0410} \mu_l^{0.0550} {D_p}^{-0.268} D_c^{-0.0330} (\rho_s - \rho_l)^{-0.316} \quad (13)$$

From Eq. 13, the bed porosity can be calculated based on factors such as slurry concentration (φs), gas velocity, liquid velocity, liquid viscosity, column diameter, particle diameter, and particle density. For this experiment, the bed porosity can be expressed as Eq. 14.

$$\varepsilon = f(\varphi_s, V_l, V_g, \mu_l, D_p, D_c, \rho_s, \rho_l) \quad (14)$$

In this experiment, liquid viscosity, particle size, column diameter, slurry concentration, gas density, and particle density were considered constants. Therefore, Eq. 14 simplifies to Eq. 15 and Eq. 16.

$$\varepsilon = f(V_l, V_g) \quad (15)$$

$$\varepsilon = a[V_l]^b \cdot [V_g]^c \quad (16)$$

Using the experimental data as model inputs, the coefficients and constants of the equations were calculated through multiple linear regression analysis, resulting in a semiempirical model of the form 17.

$$\boldsymbol{\varepsilon} = 1.31(V_l)^{0.425} \cdot (V_g)^{0.025} \quad (17)$$

Fig. 12 compares the bed expansion ratio obtained experimentally with the values predicted by model 14, while Table 4 summarizes the statistical indicators from the multiple linear regression analysis. As observed in Fig. 11, within the investigated experimental range, the predicted values closely match the measured data. The new model shows a high level of predictive accuracy, indicated by a correlation coefficient squared R2 of 0.993 and a sum of squared errors (SSE) nearly zero. These results confirm that the model reliably captures the influence of experimental parameters on bed expansion behaviour.

Table 4. Indices of model 14 multiple linear regression analysis

Serial number	Project name (abbreviated)	numerical value
1	Mean Square Error (RMSE)	0.003490
2	Sum of residuals (SSE)	0.000535
3	Correlation coefficient (R)	0.996698
4	Square of correlation coefficient (R^2)	0.993408
5	Decision Coefficient (DC)	0.993407
6	chi-square (math.)	0.000437
7	F-statistic (F-statistic)	6329.375

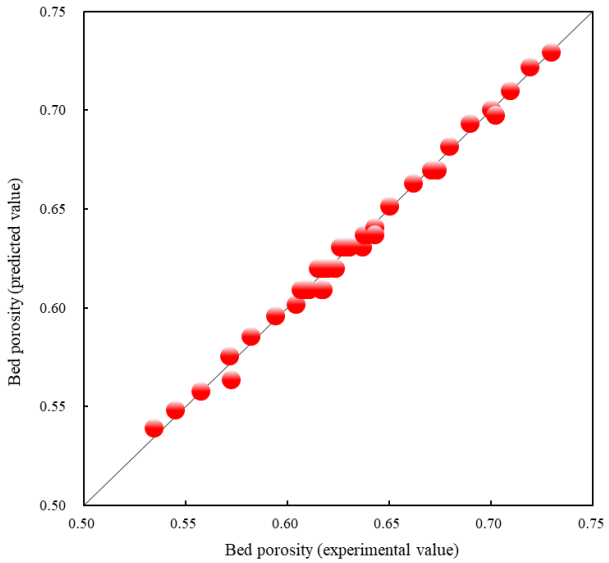

Fig. 12. Comparison of experimental results and calculated porosity of the bed

3.2.3. Standard model of dimensionless numbers for turbulence-regulated particle fluidized beds

In the previous subsection, we modelled the fluidized bed expansion ratio, fluctuation ratio, and bed porosity. The first two models are consistent in magnitude, while the bed porosity model, although predictive, is empirical and inconsistent in magnitude. Based on this experimental system, the proposed fluidized bed flow models, including gas content model 8 (models 7, 12, and 14), predict the relevant parameters well. However, these models are complex and less logical in structure. In this subsection, a suitable fluidized bed flow model for this system will be developed based on magnitude analysis, considering the factors influencing the fluidized bed flow.

Taking the bed fluctuation ratio model as an example, the influencing variables include: column diameter, apparent liquid velocity, apparent gas velocity, particle density and size, liquid viscosity, and gravitational acceleration. The bed fluctuation ratio can be expressed as.

$$r = f\left(V_l, V_g, V_{so}, D_c, D_p, H_0, \mu_l, \rho_l, \rho_s, g\right) \tag{15}$$

The above experimental influences were analyzed in terms of magnitude, and the appropriate dimensionless group was chosen for modeling based on the analysis results. To make the proposed model concise and efficient, three-dimensional dimensionless numbers were selected to represent the effects of liquid Reynolds number16 and gas Froude number 17, reflecting the liquid and gas phases.

$$Re_l = \frac{\rho_l \cdot V_l \cdot D_c}{\mu_l} \tag{16}$$

$$Fr_g = \frac{{V_g}^2}{D_c \cdot g} \tag{17}$$

To analyze the effect of solid-phase filling particles, we have attempted to derive a dimensionless number representing the ratio of solid-phase to bed fluctuation using Buckingham's Theorem (π Theorem) in quantitative analysis.

Based on the experimental analysis, several physical parameters of solid-phase particles are identified as potentially influencing the fluidization process. These include the particle diameter D_p, the ratio between the flotation column diameter D_p and particle size D_p, the initial static bed height H0, which reflects the quantity of solid-phase particles, the terminal settling velocity V_{so} that characterizes particle interference during sedimentation, the particle density ρs, and gravitational acceleration g. Accordingly, the number of influencing variables n is determined to be 6. The corresponding functional relationship is therefore expressed as shown in Eq. 18.

$$f\left(D_p,\ V_{so},\ \rho_{s,}\ D_c,\ H_0,\ g\right) = 0 \tag{18}$$

According to the principle of basic quantity determination in this study, the particle size of solid-phase particles D_p, the interference settling end velocity of solid-phase particles during fluidization Vso and the density of solid-phase particles ρ_s are taken as the basic quantities, and then the basic quantity m is equal to 3. The number of phases (π terms) of the scale of unity, the π number N is:

$$N(\pi) = n - m = 6 - 3 = 3$$

$$\pi_1 = D_p^{a1} \cdot V_{S0}^{b1} \cdot \rho_s^{c1} \cdot D_c$$

$$\pi_2 = D_p^{a2} \cdot V_{S0}^{b2} \cdot \rho_s^{c2} \cdot H_0$$

$$\pi_3 = D_p^{a3} \cdot V_{S0}^{b3} \cdot \rho_s^{c3} \cdot g$$

The indices of each π-term are determined based on the principle of measure harmony, and the three basic measures used are length (L), mass (M), and time (T), which are respectively substituted into the π-term.

Then for π_1 we have:

$$dim\pi_1 = dim\ (D_p^{a1} \cdot V_{S0}^{b1} \cdot \rho_s^{c1} \cdot D_c)$$

imitate:

$$M^0L^0T^0 = (L)^{a1} \cdot (L \cdot T^{-1})^{b1} \cdot (M \cdot L^{-3})^{C1} \cdot (L)$$

$$M\colon 0 = c_1$$

$$L\colon 0 = a_1 + b_1 - 3c_1 + 1$$

$$T\colon 0 = -b_1$$

catch (a disease):

$$a_1 = -1,\ b_1 = 0,\ c_1 = 0,\ \pi_1 = \frac{D_c}{D_p}$$

The same reasoning can be used to obtain:

$$\pi_2 = \frac{H_0}{D_p},\ \pi_3 = \frac{D_{p\cdot g}}{V_{S0}^2}$$

Substituting the π term into the π-theorem equation (4-x1) yields the equation (4-x):

$$f_1\left(\frac{D_c}{D_p},\ \frac{H_0}{D_p},\ \frac{D_{p\cdot g}}{V_{S0}^2}\right) = 0 \tag{19}$$

According to the need of solving, it can be seen that the required functional equation is a dimensionless set, and the three π terms in Eq. 19 are dimensionless numbers, then according to the relevant conversion of π theorem, we can finally get Eq. 20 to represent the dimensionless number of solid-phase particles' influence on the parameters of fluidized bed hydrodynamics, which is expressed in Sp, as follows:

$$Sp = \frac{D_c \cdot H_0 \cdot g}{D_p \cdot V_{S0}^2} \tag{20}$$

In this experiment, the dimensionless Sp number ranges from 15 to 80, corresponding to different fluidization states. When Sp is less than 30, the particle size is small and the bed height is low, leading to weak constraint of solid particles by convective transport. The bed fluctuation ratio exceeds 1.4, indicating a violently fluctuating fluidization state. When Sp is between 30 and 60, the particle constraint is moderate, with a fluctuation ratio of 1.1–1.4 and an expansion ratio of 1.2–1.6, which is the stable fluidization state commonly used in industrial flotation. When Sp is greater than 60, the particle size is large and the bed height is high, resulting in strong particle constraints. The fluctuation ratio is less than 1.1 and the expansion ratio is less than 1.2, representing a dense fluidization state that is prone to particle deposition. This classification provides a practical reference for the selection of operating parameters in industrial fluidized beds.

Then the bed fluctuation ratio model can be expressed as Eq. 21, the:

$$r = a \cdot [Re_l]^b \cdot \left[Fr_g\right]^c \cdot [Sp]^d \tag{21}$$

Multiple linear regression was applied to estimate the coefficients and constants, which were then substituted into Eq. 21 to derive Eq. 22:

$$r = 24.1(Re_l)^{-0.309} \cdot \left(Fr_g\right)^{-0.00349} \cdot (Sp)^{-0.173} \tag{22}$$

Fig. 13 illustrates the bed fluctuation ratio. Experimental values are compared with the calculated values from Eq. 22. In Fig. 13, R^2 is 0.923 and SSE is 0.003, which indicates that the changes in bed fluctuations of the experimental variables within the studied range of parameters can be accurately predicted within that range.

Similarly, expansion ratio model Eq. 23, porosity model Eq. 24, and gas content model Eq. 25:

$$R = 9.60E-06(Re_l)^{1.29} \cdot \left(Fr_g\right)^{0.0375} \cdot (Sp)^{0.214} \tag{23}$$

$$\varepsilon = 8.79E-03(Re_l)^{0.466} \cdot \left(Fr_g\right)^{0.0138} \cdot (Sp)^{0.0176} \tag{24}$$

$$\varepsilon_g = 1.43E-04(Fr_g)^{0.466} \cdot (Re_l)^{0.959} \cdot \left(\frac{V_l}{V_{so}}\right)^{2.80} \cdot \left(\frac{H_o}{D_c}\right)^{0.864} \tag{25}$$

Models 22, 23, 24 and 25 can be seen in Fig. 13 and Table 5 to be effective in predicting the relevant parameter values. The dimensionless flow model of a fluidized bed can be unified in the form of Eq. 26:

$$K = a[Re_l]^b \cdot \left[Fr_g\right]^c \cdot [Sp]^d \tag{26}$$

3.3. Correlation between bubble diameter and bed expandability in turbulence regulated particle fluidized beds

The gas phase moves through the fluidized bed as bubbles, and the variation in bubble characteristics is strongly linked to bed expansion behaviour. In this subsection, we examine how bubble dynamics interact with expansion features of the bed to better understand the mechanism of bubble formation.

3.3.1. Correlation study between bubble diameter and bed expansion parameters

Fig. 14 illustrates how bubble diameter varies with fluctuation ratio, expansion ratio, and porosity at different initial bed heights. From the figures, it is clear that bubble size shows two distinct patterns depending on bed height: when the initial bed height is below 0.290 m, the diameter increases rapidly as the expansion parameter grows; when it is above 0.290 m, the growth becomes more gradual. This suggests that bubble size is heavily affected by bed expansion conditions. Additionally, as bed height increases, bubble behavior tends to stabilize. Therefore, the initial bed height acts as a key factor connecting gas–liquid dynamics with bed expansion behavior, influencing the interaction between bubbles and the bed.

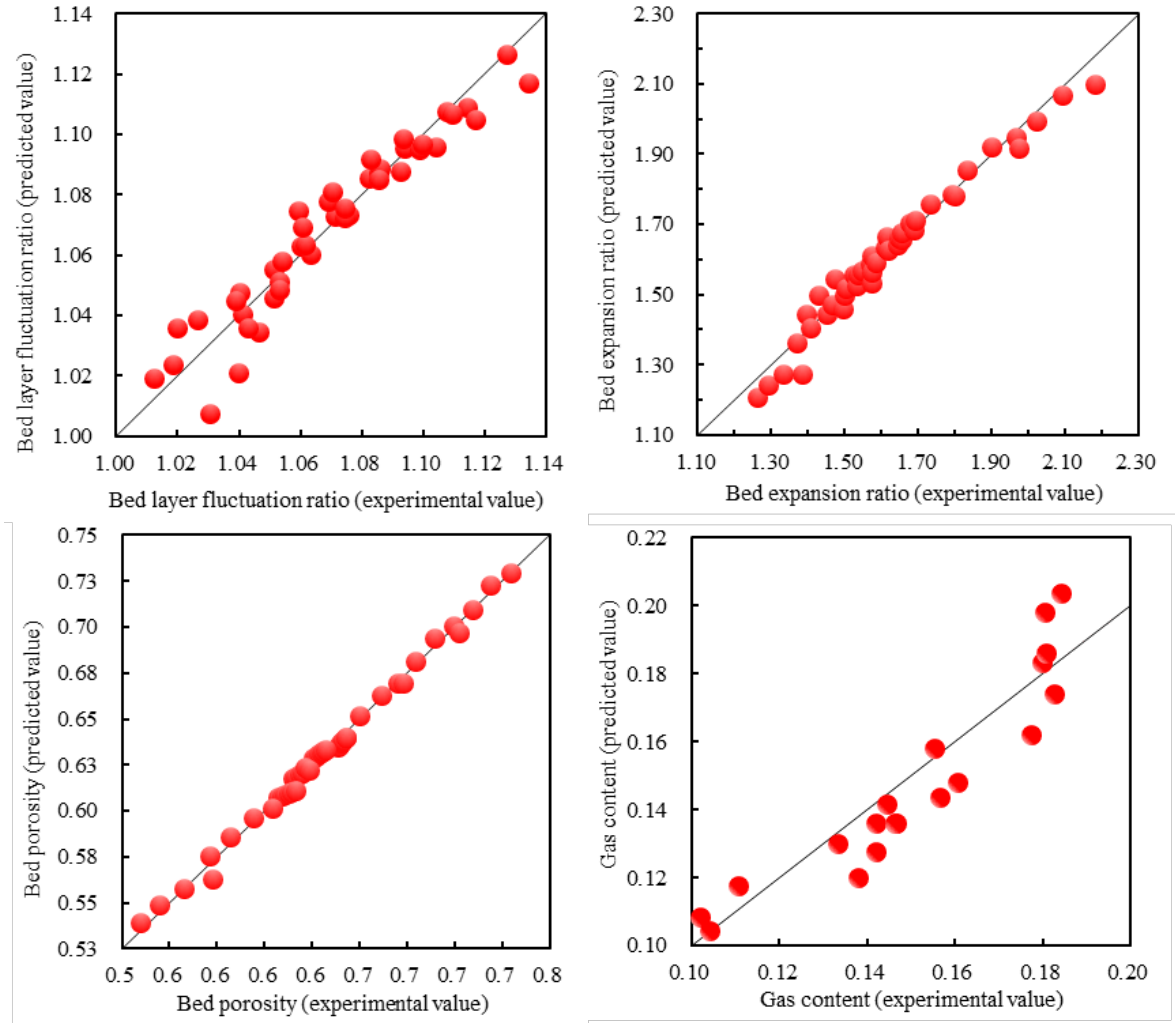

Fig. 13. Comparison of predicted and correlated experimental values for models 22, 23, 24 and 25

Table 5. Multiple linear regression analysis indices for models 22, 23, 24 and 25

Serial number	Project Name (abbreviated)	Style 22	Style 23	Style 24	Style 25
1	RMSE	0.008268	0.036650	0.003155	0.003254
2	SSE	0.003007	0.059104	0.000438	0.046607
3	R	0.960628	0.984261	0.997303	0.987478
4	R2	0.922806	0.968770	0.994613	0.975113
5	DC	0.922802	0.968648	0.994613	0.974993
6	Chi-square	0.001425	0.019415	0.000358	0.015310
7	F Statistic	502.0844	1302.860	7755.574	1645.672

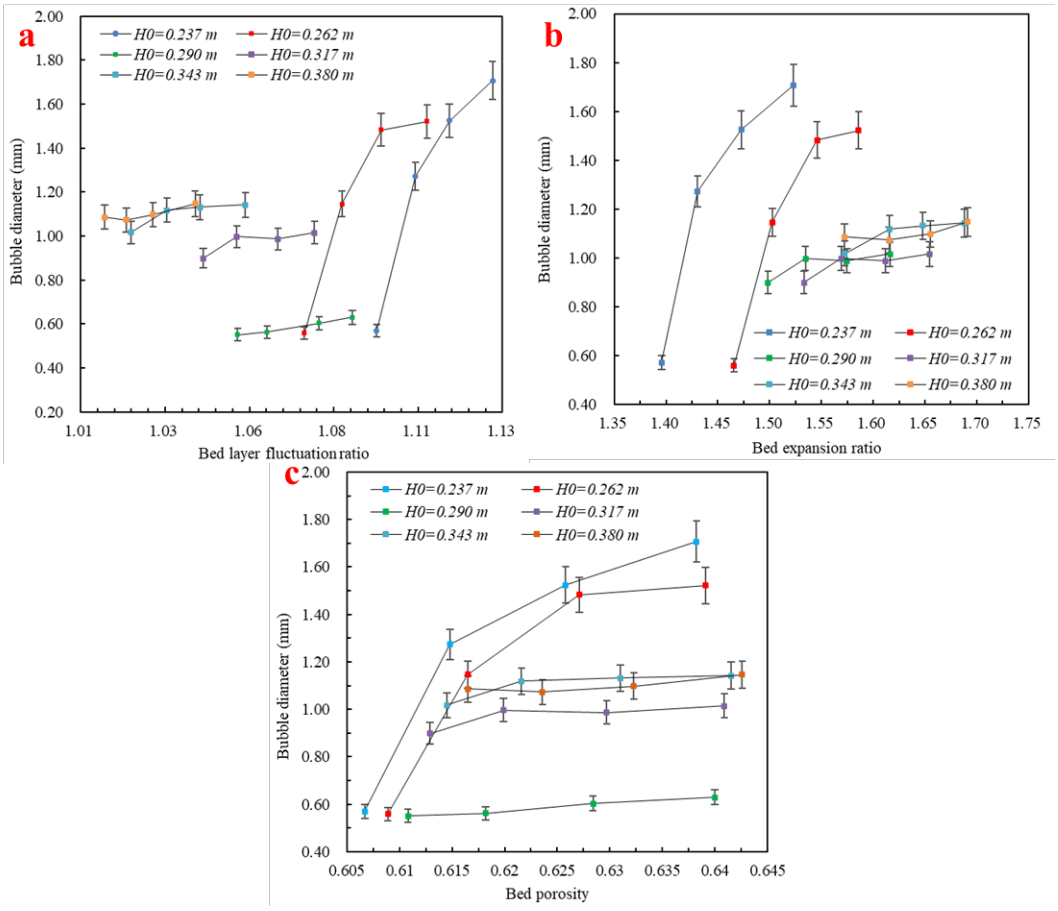

Fig. 14. (a) Variation of bubble diameter versus bed fluctuation ratio. (b) Variation relationship between bubble diameter and bed expansion ratio. (c) Variation relationship between bubble diameter and bed porosity

3.3.2. Exploration of bubble diameter prediction in turbulence-regulated particle fluidized beds

The previous subsection examined the connection between bubble size and bed expansion parameters, concluding that the initial bed height is the main factor affecting bubble diameter changes. This subsection will further explore the prediction model for bubble diameter, using the initial bed height as the key condition.

The primary experimental factors affecting bubble size are superficial gas velocity, liquid velocity, initial bed height, and column diameter. Using these parameters, the bubble diameter can be represented as Eq. 27:

$$D_b = f\left(V_l, V_g, V_{so}, D_c, D_p, H_0, \mu_l, \rho_l, \rho_s, g\right) \tag{27}$$

Building on the previous analysis of bubble diameter and bed swelling parameters, model fitting was conducted using experimental data. After detailed calculations, the findings indicate that bubble size is primarily governed by four dimensionless groups, as expressed in Eq. 28, while Eq. 29 is applied for model fitting to normalize the model's scale.

$$D_b = f\left(Fr_g, r, R, \varepsilon\right) \tag{28}$$

$$\frac{D_b}{D_C} = a[Fr_g]^b \cdot [r]^c \cdot [R]^d \cdot [\varepsilon]^e \tag{29}$$

The coefficients and constants were determined through multiple linear regression, taking the static bed height as the key condition, and Eq. 30 was obtained as follows.

$$\frac{D_b}{D_C} = \begin{cases} 2.36E-31\left(Fr_g\right)^{0.319}(r)^{80.2}(R)^{35.8}(\varepsilon)^{-114}, & H_o < 0.290\ m \\ 5.56E-07\left(Fr_g\right)^{0.050}(r)^{-6.17}(R)^{8.57}(\varepsilon)^{-15.1}, & H_o \geq 0.290\ m \end{cases} \tag{30}$$

Fig. 15 shows the comparison between predicted and observed bubble diameters from model 30, while Table 6 lists the regression coefficients. The results demonstrate that when the bed height is below

0.290 m, the fitted R2 value reaches 0.985, and when the bed height is above 0.290 m, the R2 is 0.921. Within this parameter range, the predictions of Eq. 30 align well with the experimental data. This confirms that, across different initial bed heights, the model can effectively capture variations in bubble diameter.

Table 6. Model 30 multiple linear regression analysis indices

Serial number	Project name (abbreviated)	H0 < 0.290 m	H0≥ 0.290 m
1	RMSE	1.005114	0.0015968
2	SSE	8.082034	9.17927E-5
3	R	0.992529	0.9598969
4	R2	0.985113	0.9214022
5	DC	0.985109	0.9214810
6	Chi-square	0.259531	0.0027477
7	F Statistic	397.0461	193.7922

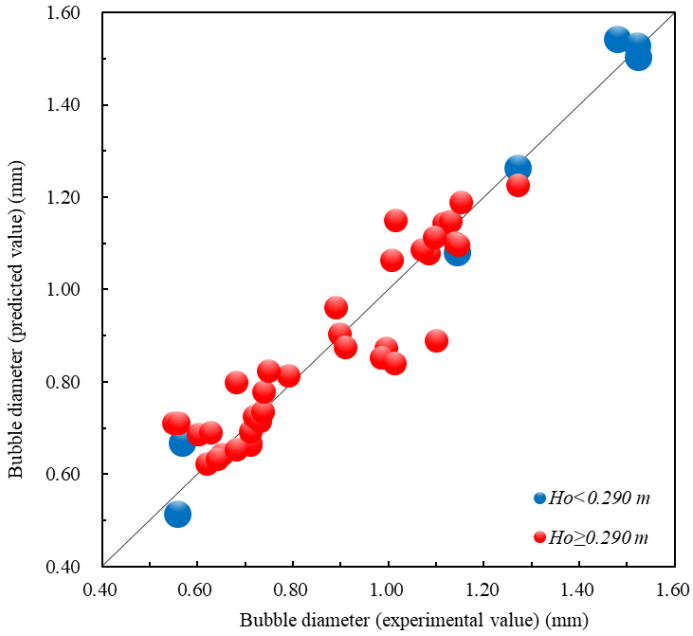

Fig. 15. Comparison of measured and predicted bubble diameters at different static bed heights

4. Conclusions

This chapter explores the fluidization characteristics of a turbulence-controlled particulate flotation column, focusing on how experimental factors affect pressure drop and the changes in expansion-related parameters such as fluctuation ratio, expansion ratio, and porosity. A model for bed flow parameters was developed using magnitude analysis combined with multiple linear regression, and the dimensionless flow parameter model (based on a single particle size of the filled medium) was unified. The main conclusions are:

(1) When the particle size of the filler is the same, the initial bed height does not affect the minimum fluidization velocity of the system. Under the same particle density, larger particles require a lower velocity for fluidization. For other experimental conditions, a higher gas flow rate at the point of fluidization onset results in a smaller minimum velocity. Within a fixed bed height, the minimum fluidization velocity varies linearly with the apparent gas velocity, showing a decreasing trend as the gas velocity increases.

(2) When particles with high density and large size are used as filling particles, the expansion characteristic parameters of the fluidized bed experience small changes, and the parameter curves change gradually; in this experimental setup, the changes in bed expansion ratio and bed porosity within the expansion characteristic parameters are positively correlated.

(3) With 3 mm steel beads as the filler, the proposed fluctuation ratio model, expansion ratio model, and empirical porosity model align well with experimental observations and remain within the scope of the conducted studies. The models are presented as follows.

$$r = 0.565(Re_l)^{0.106} \cdot \left(\frac{V_l}{V_{so}}\right)^{-0.036} \cdot \left(\frac{V_g}{V_{so}}\right)^{0.015} \cdot \left(\frac{H_o}{D_c}\right)^{-0.174}$$

$$R = 0.001(\frac{G_f}{G_{mf}})^{0.58} \cdot (\frac{H_s}{D_c})^{-0.735} \cdot \left(\frac{D_{pav}}{D_c}\right)^{-2.02} \cdot \left(\frac{\rho_s}{\rho_f}\right)^{-0.14}$$

$$\varepsilon = 1.31(V_l)^{0.425} \cdot \left(V_g\right)^{0.025}$$

(4) The flow model is developed using the liquid Reynolds number and the gas Fred's number to represent the influence of the liquid and gas phases on the flow characteristics, respectively. Additionally, a dimensionless number Sp is introduced to represent the effect of filled particles on the flow parameters by applying Buckingham's theorem in the magnitude analysis method. This approach integrates the dimensionless number model within the flow model of a three-phase fluidized bed. The new model shows excellent predictions of gas expansion parameters and the gas content rate. The liquid Reynolds number, gas Fred's number, dimensionless number Sp, and the new model are summarized as follows.

$$Re_l = \frac{\rho_l \cdot V_l . D_c}{\mu_l}$$

$$Fr_g = \frac{{V_g}^2}{D_c \cdot g}$$

$$Sp = \frac{D_c \cdot H_0 . g}{D_p \cdot V_{S0}^2}$$

$$K = a[Re_l]^b \cdot \left[Fr_g\right]^c \cdot [Sp]^d$$

(5) When the initial bed height is below 0.290 m, bubble diameter increases rapidly with rising bed expansion parameter; whereas when the bed height exceeds 0.290 m, the bubble size grows more slowly under the same parameter change. The initial bed height influences how bubbles interact with the bed's expansion characteristics. The proposed prediction model aligns well with the experimental results.

$$\frac{D_b}{D_C} = \begin{cases} 2.36E-31\left(Fr_g\right)^{0.319}(r)^{80.2}(R)^{35.8}(\varepsilon)^{-114}, & H_o < 0.290\ m \\ 5.56E-07\left(Fr_g\right)^{0.050}(r)^{-6.17}(R)^{8.57}(\varepsilon)^{-15.1}, & H_o \geq 0.290\ m \end{cases}$$

Acknowledgments

This paper is supported by the Fundamental Research Funds for the National Natural Science Foundation of China (Grant No. 51874884) and we also want to thank the support of the Key Science and Technology Projects of China National Coal Group Corp (20231CY003).

References

Abu KHALIFEH, H., MADHURANTHAKAM, C.M., DHIB, R., 2021. *Empirical models for the hydrodynamics of turbulent bed contactor with non-Newtonian liquids: (part 3)*. Chem. Eng. Commun. 208(1), 110-125.

AOYAMA, S., HAYASHI, K., HOSOKAWA, S., TOMIYAMA, A., 2016. *Shapes of ellipsoidal bubbles in infinite stagnant liquids*. Int. J. Multiph. flow 79, 23-30.

BESAGNI, G., INZOLI, F., 2019. *Bubble sizes and shapes in a counter-current bubble column with pure and binary liquid phases*. Flow Meas. Instrum. 67, 55-82.

BHUNIA, K., KUNDU, G., MUKHERJEE, D., 2015. *Statistical model for gas holdup in flotation column in presence of minerals*. Can. Metall. Q. 54(2), 235-246.

CAI, X.L., CHEN, J.Q., LIU, M.L., JI, Y.P., AN, S., 2017. *Numerical studies on dynamic characteristics of oil-water separation in loop flotation column using a population balance model*. Sep. Purif. Technol. 176, 134-144.

DORA, D.T.K., MOHANTY, Y.K., ROY, G.K., SARANGI, B., 2014. *Prediction of bed fluctuation and expansion ratios for homogeneous ternary mixtures of spherical glass bead particles in a three-phase fluidised bed*. Can. J. Chem. Eng. 92(3), 536-542.

ELLINGSEN, K., RISSO, F., 2001. *On the rise of an ellipsoidal bubble in water: oscillatory paths and liquid-induced velocity*. J. Fluid Mech. 440, 235-268.

FAN, M.M., TAO, D., ZHAO, Y.M., HONAKER, R., 2013. *Effect of nanobubbles on the flotation of different sizes of coal particle*. Miner. Metall. Process. 30(3), 157-161.

GORAIN, B.K., FRANZIDIS, J.P., MANLAPIG, E.V., 1999. *The empirical prediction of bubble surface area flux in mechanical flotation cells from cell design and operating data*. Miner. Eng. 12(3), 309-322.

JENA, H.M., ROY, G.K., MEIKAP, B.C., 2008a. *Prediction of gas holdup in a three-phase fluidized bed from bed pressure drop measurement. chem*. Eng. Res. Des. 86(11A), 1301-1308.

JENA, H.M., SAHOO, B.K., ROY, G.K., MEIKAP, B.C., 2008b. *Characterization of hydrodynamic properties of a gas-liquid-solid three-phase fluidized bed with regular shape spherical glass bead particles*. Chem. Eng. J. 145(1), 50-56.

JO, Y.B., PARK, S.H., YOO, H.S., KIM, E.S., 2022. *Gpu-based SPH-DEM Method to Examine the Three-Phase Hydrodynamic Interactions between Multiphase Flow and Solid Particles*. Int. J. Multiph. flow 153.

LEFEBVRE, S., GUY, C., CHAOUKI, J., 2007. *Solid phase hydrodynamics of three-phase fluidized beds - A convective/dispersive mixing model*. Chem. Eng. J. 133(1-3), 85-95.

LEI, W., ZHANG, M., ZHANG, Z.X., ZHAN, N., FAN, R., 2020. *Effect of bulk nanobubbles on the entrainment of kaolinite particles in flotation*. Powder Technol. 362, 84-89.

LI, Y.R., LI, Q., YANG, J.M., ZHOU, X.M., YIN, X.M., ZHAO, D.M., 2008. *Expression patterns of Doppel gene in golden hamster: Quantification using real-time RT-PCR*. Mol. Cell. Probes. 22(4), 255-258.

LIU, L., ZHANG, H.Y., YAN, H.J., ZIEGENHEIN, T., HESSENKEMPER, H., ZHOU, P., LUCAS, D., 2021. *Experimental studies on bubble aspect ratio and corresponding correlations under bubble swarm condition*. Chem. Eng. sci. 236.

LOTH, E., 2008. *Quasi-steady shape and drag of deformable bubbles and drops*. Int. J. Multiph. Flow. 34(6), 523-546.

PAN, H., LI, Y.F., LI, N.B., GAO, F.L., FU, X.Q., ZHU, R.T., EVANS, G., 2018. *Study on gas holdup in a fluidized flotation column from bed pressure drop*. Energ. Sources. 40(14), 1693-1671

RAVICHANDRAN, V., ESWARAIAH, C., SAKTHIVEL, R., BISWAL, S.K., MANISANKAR, P., 2013. *Gas dispersion characteristics of flotation reagents*. Powder Technol. 235, 329-335.

SARHAN, A.R., NASER, J., BROOKS, G., 2017. *CFD analysis of solid particles properties effect in three-phase flotation column*. Sep. Purif. Technol. 185, 1-9.

SHI, W.B., YANG, J., LI, G., YANG, X.G., ZONG, Y., CAI, X.Y., 2018. *Modelling of breakage rate and bubble size distribution in bubble columns accounting for bubble shape variations*. Chem. Eng. Sci. 187, 391-405.

SIVAIAH, M., MAJUMDER, S.K., 2013. *Hydrodynamics and mixing characteristics in an ejector-induced downflow slurry bubble column (EIDSBC)*. Chem. Eng. J. 225, 720-733.

SOBRINO, C., Almendros-Ibáñez, J.A., SANTANA, D., Vázquez, C., de VEGA, M., 2009. *Maximum entropy estimation of the bubble size distribution in fluidized beds*. Chem. Eng. Sci. 64(10), 2307-2319.

VENKATRAMAN, P.Z., 1996. *Evaluation of an advanced fine coal cleaning circuit*.

WANG, G.C., GE, L.H., MITRA, S., EVANS, G.M., JOSHI, J.B., CHEN, S.Y., 2018. *A review of CFD modelling studies on the flotation process*. Miner. Eng. 127, 153-177.

WANG, T.F., WANG, J.F., YANG, W.G., JIN, Y., 2003. *Experimental study on bubble behavior in gas-liquid-solid three-phase circulating fluidized beds.* Powder Technol. 137(1-2), 83-90.

YIANATOS, J., VINNETT, L., PANIRE, I., Alvarez-SILVA, M., Díaz, F., 2017. *Residence time distribution measurements and modelling in industrial flotation columns.* Miner. Eng. 110, 139-144.